Angle-resolved ultraviolet photoelectron spectroscopy and theoretical simulation of a well-ordered ultrathin film of tetratetracontane (n-$C_{44}H_{90}$) on Cu(100): Molecular orientation and intramolecular energy-band dispersion

Daisuke Yoshimura, Hisao Ishii, and Yukio Ouchi
Department of Chemistry, Graduate School of Science, Nagoya University, Furo-cho, Chikusa-ku, Nagoya 464-8602, Japan

Eisuke Ito
Venture Business Laboratory, Nagoya University, Furo-cho, Chikusa-ku, Nagoya 464-8603, Japan

Takayuki Miyamae and Shinji Hasegawa
Institute for Molecular Science, Myodaiji-cho, Okazaki 444-8585, Japan

Koji Kamiya Okudaira
Department of Materials Science, Faculty of Engineering, Chiba University, Yayoi-cho, Inage-ku, Chiba 263-8522, Japan

Nobuo Ueno
Department of Materials Technology, Faculty of Engineering, Chiba University, Yayoi-cho, Inage-ku, Chiba 263-8522, Japan and Institute for Molecular Science, Myodaiji-cho, Okazaki 444-8585, Japan

Kazuhiko Seki
Research Center for Materials Science and Department of Chemistry, Graduate School of Science, Nagoya University, Furo-cho, Chikusa-ku, Nagoya 464-8602, Japan

(Received 5 April 1999)

The electronic structure and molecular orientation of a tetratetracontane (n-$C_{44}H_{90}$; TTC) ultrathin film on a Cu(100) surface were studied by angle-resolved ultraviolet photoelectron spectroscopy (ARUPS) using synchrotron radiation. A well-oriented thin film of TTC was successfully prepared by vacuum evaporation in ultrahigh vacuum at room temperature. We observed a (2×1)-like low-energy electron-diffraction (LEED) pattern for the deposited TTC film. This result indicates that the TTC molecules lie on the Cu(100) surface in two types of domains, rectangular to each other, in which the alkyl-chain axes are along the [110] and $[1\bar{1}0]$ directions of the Cu(100) surface. The application of the dipole selection rules to the normal-emission ARUPS spectrum revealed that the C—C—C plane of TTC is parallel to the Cu(100) surface plane (flat-on orientation). The intramolecular energy-band dispersion of TTC was examined by changing the take-off angle of emitted electron along the [110] direction of the Cu(100) surface. The observed results support the conclusion about the direction of alkyl-chain axes by LEED observation. In order to analyze the molecular orientation more quantitatively, we also performed theoretical simulations of the angle-resolved photoemission spectra using the independent-atomic-center (IAC) approximation combined with *ab initio* molecular-orbital (MO) calculations for various molecular orientations. The simulated spectra for flat-on orientation are in excellent agreement with the observed spectra. These results once again verify the deduced molecular orientation, and also demonstrate the reliability of theoretical simulation with the IAC/MO approximation for compounds without a π-electron system. Furthermore, we observed a work function change of about -0.3 eV by adsorption of TTC. Such a decrease of the work function indicates the formation of a dipole layer at the interface, in contrast to the traditional picture of energy-level alignment assuming a common vacuum level at the organic/metal interface. [S0163-1829(99)13735-4]

I. INTRODUCTION

Polyethylene is one of the prototype polymers and also a typical quasi-one-dimensional compound. Its electronic structure has been studied extensively, since the elucidation of its electronic structure is important not only because it is of fundamental interest but also because it forms the basis for understanding the electronic structure of many derivative polymers. For polymers which consist of regularly repeating units, we can expect the formation of intrachain one-dimensional bands with an energy-band dispersion relation $E=E(\mathbf{k})$ between the energy E and wave number $\mathbf{k}$ of an electron. Studies of such relations can be performed using oriented polymer samples by angle-resolved ultraviolet photoelectron spectroscopy (ARUPS).[1] For practical studies of the intrachain one-dimensional band structure of polyethylene by ARUPS, long-chain n-alkanes have been used as good model compounds, since very well-oriented samples can be prepared by vacuum deposition.[2]

In Fig. 1 we schematically show the three typical orientations for n-alkanes. For these orientations, there are two modes of ARUPS measurements for observing such energy-

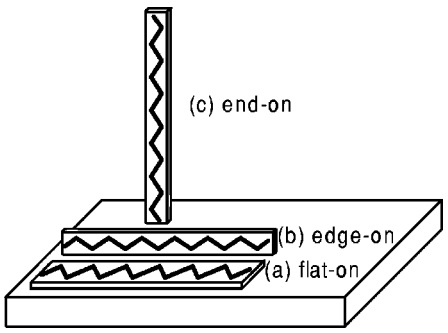

FIG. 1. Schematic view of the three typical orientation models for *n*-alkane: (a) flat-on orientation, (b) edge-on orientation, and (c) end-on orientation. In the end-on orientation the alkyl-chain axes are perpendicular to the substrate surface. In the case of flat-on and edge-on orientations, the alkyl-chain axes are parallel to the substrate surface, and their C—C—C planes are parallel and perpendicular to the substrate surface, respectively.

band dispersion.[3,4] One (a) is a normal-emission measurement with changing incident photon energy for the end-on oriented sample, where the alkyl-chain axes are along the surface normal direction. The other (b) is measurements scanning the take-off angle, with a fixed incident photon energy for the parallel-oriented sample, where the alkyl-chain axes are parallel to the surface, as realized in the flat-on and edge-on orientations. The principle of band mapping in these two modes will be described later in Sec. III.

The measurements of end-on oriented samples [mode (a)] have been reported for various systems: hexatriacontane [n-$CH_3(CH_2)_{34}CH_3$; HTC] on an oxidized Cu plate,[5–8,10] a Langmuir Blodgett film of Ca-arachidate,[8] pentatriacontane-18-one [$CH_3(CH_2)_{16}CO(CH_2)_{16}CH_3$],[9] and a self-assembled monolayer (SAM) film of docosanethiol [$CH_3(CH_2)_{21}SH$].[10]

As shown in Sec. III, however, in mode (a) we have to make some assumption about the final state of the excited electron. A free-electron-like parabolic relation is often assumed with a constant inner potential V_0[1,3,4] as an adjustable parameter of the energy position of this parabola. The value of V_0 was experimentally estimated by the $h\nu$ dependence of the photoemission intensity of the C $2s$ band,[8] but there still remains some ambiguity. In Ref. 8, the effective mass of an excited electron m^* was assumed by the free-electron mass m_0 ($m^*/m_0=1$), but the results of low-energy electron transmission (LEET) experiments on long-chain alkanes[11,12] at low-energy region (<15 eV) did not support this assumption. Therefore, we need further discussion on this point.

On the other hand, in mode (b), there is no ambiguity as in mode (a). Therefore, the measurement with mode (b) is more ideal for the investigation of energy-band dispersion. Unfortunately, however, its application to polymers has been limited to the topmost valence band of polydiacetylene film grown,[13] and the preliminary results for $(SN)_x$ (Ref. 14) using a single crystal. This limitation is due to the difficulty of preparing a highly oriented thin film for avoiding sample-charging problem in ultraviolet photoemission spectroscopy measurements. If we can prepare parallel-oriented film of an *n*-alkane molecule with its axis azimuthally aligned along a particular direction, it enables us to determine the band structure more precisely with mode (b) than mode (a). In addition, in order to examine the complete energy-band structure, a measurement with both modes is desired from the viewpoint of the selection rules: the bands forbidden in mode (a) are often allowed in mode (b), and vice versa.

In order to perform the experiment with mode (b), the preparation of a parallel-oriented (e.g., flat-on and edge-on in Fig. 1) film is required. Such orientations, were found in some reports for several *n*-alkanes by the techniques such as low-energy electron diffraction (LEED),[15,16] near-edge *x*-ray absorption fine structure,[17] Penning ionization electron spectroscopy,[18,19] scanning tunneling microscopy,[20–22] and infrared reflection absorption spectroscopy (IR-RAS).[23–26] In these studies, clean surfaces of highly oriented pyrolitic graphite (HOPG) or a (111) surface of transition-metal single crystals with sixfold symmetry were used as the substrates. The conclusions for molecular orientation in these studies were flat-on in Refs. 15, 16, 18–20, and 23–26, and edge-on in Refs. 17, 21, and 22.

For ARUPS, Dudde and Reihl reported a study of the system of hexatriacontane (n-$C_{36}H_{74}$; HTC)/Cu(111).[27] Between the two types of parallel orientation, they concluded edge-on orientation by applying the selection rules to the observed ARUPS spectrum. However, Weckesser *et al.*[28] pointed out that these selection rules were in error, and the application of the corrected selection rules to the same data for HTC/Cu(111) gave a flat-on orientation.

In spite of the success in preparing the HTC film with parallel orientation on Cu(111), the energy-band dispersion along the molecular axis of HTC had not been reported. This was probably because of the complicated domain structure of the HTC film expected from the sixfold symmetry of the Cu(111) substrate. By using substrates with fourfold symmetry such as the (100) surface, and taking account of the twofold symmetry of the *n*-alkane molecule, we can expect the possibility of realizing a two-domain structure, which makes the measurements and analysis in mode (b) easier. In addition, the comparison of molecular orientations between (111) and (100) surfaces is also interesting.

In order to observe energy-band dispersion along the alkyl-chain direction, a precise estimation of the molecular orientation is necessary, and especially the direction of the alkyl chain should be known. Although the application of the selection rules is simple and convenient, it leads to only a qualitative conclusion among possible geometries like those in Fig. 1, and we cannot exclude the possibility of the tilting of alkyl-chain axis or C—C—C plane from the substrate surface in the real systems. There are some trials to estimate the tilting angle of the alkyl chain for an end-on oriented sample.[10,29,30] However, no quantitative examination of the tilt of the alkyl chain or the C—C—C plane for a parallel-oriented sample has been performed.

The quantitative simulation of the emission intensity of ARUPS spectra is expected to offer the possibility of obtaining further detailed information for molecular orientation. First, the comparison of the observed ARUPS spectra with reliable simulation allows detailed assignments of spectral features based on their intensity for samples with known or random geometry. Second, it becomes possible to analyze the spectra for any geometry and emission angle quantitatively. Thus we can predict how the spectra depend on the emission angles for a given molecular geometry, including

the simulation of the spectra taken for determining the energy-band dispersion relation. Further, we can now estimate the molecular orientation with full freedom of the molecular geometry by the comparison with simulations with various geometries.

Until recently, no simple and effective theoretical model was available for the analysis of photoelectron angular distribution of such large functional organic films. We have developed such a theoretical method of calculating the ARUPS intensity from large molecules based on the independent-atomic-center (IAC) approximation.[31,32] In this approximation, the photoelectron wave function is approximated by a coherent sum of the electron waves emitted from atomic orbitals which build up the molecular orbital, where the contribution of the waves scattered by surrounding atoms is neglected. This model has been successfully applied to analyze the take-off angle (θ) and azimuthal angle (ϕ) dependencies of photoelectron intensities from oriented ultrathin films of various organic compounds, i.e., phthalocyanines on MoS_2,[33,34] bis(1,2,5-thiadiazolo)-*p*-quinobis(1,3-ditiole) on MoS_2,[35–37] tetracene on highly oriented pyrolitic graphite (HOPG),[38] perylenetetracarboxylicdianhydride on MoS_2,[39] and *p*-sexiphenyl (6P) on evaporated Ag.[40] The studies of randomly orientated systems such as the energy dependence of emission intensity from the highest occupied molecular orbital of C_{60},[41] the radiation damage of poly(methylmethacrylate),[42] poly(1,10-phenanthroline-3,8-diyl),[43] and polystyrene[44] have also been reported. Especially in Refs. 34, 37–39, 41, and 44, better correspondence between the calculation and measured spectra was achieved by considering the single scattering of photoelectrons by surrounding atoms. These studies indicated that the IAC/molecular-orbital (MO) approximation is useful in analyzing the ARUPS of oriented large organic molecules despite its simplicity. So far these studies have been limited to the planar molecules with large π conjugation, and IAC/MO calculation has not yet been applied to the materials that consist of only σ electrons. Further, the substrates used in these studies were layered compounds or evaporated metal, and the ordered organic layer prepared onto well-defined metal surface has not yet been investigated.

In this work, we studied the electronic structure and molecular orientation of a tetratetracontane (n-$C_{44}H_{90}$;TTC) ultrathin film on Cu(100) by ARUPS measurements and LEED observation. An oriented thin film of TTC was successfully prepared by vacuum evaporation in ultrahigh vacuum. By analyzing the LEED pattern and applying the dipole selection rules to the normal-emission spectra, we could determine the surface structure of TTC film on the clean Cu(100) substrate. Our conclusion for the orientation of alkyl chain is that the C—C—C plane of TTC is parallel to the Cu(100) surface plane (flat-on orientation) in two types of domains, rectangular to each other, in which the alkyl-chain axes are along the [110] and $[1\bar{1}0]$ directions of Cu(100) surface. The intramolecular band dispersion of TTC was also examined along the [110] direction and other equivalent directions of Cu(100) surface by measuring the take-off angle dependence of the ARUPS spectra. The experimentally observed band structure showed excellent correspondence to the results of previous band calculations.

We also simulated the angular dependence of photoemission intensity and peak shifts with the theoretical calculations based on IAC approximation combined with *ab initio* MO calculations. Obtained results showed excellent agreement with the observed spectra, supporting our conclusions for the orientation of a TTC thin film. This allowed a detailed analysis of the energy dispersion relation. Comparing the energy-band dispersions calculated and measured for flat-on orientation in this study with that in Ref. 8 for end-on orientation, a very good correspondence could be obtained. These results indicate that the assumption of a free-electron-like final state was reasonable, and the estimated value of the inner potential V_0 in these reports was also good. An explicit examination of the possible tilting of the chain axis and/or the C—C—C plane from the substrate surface was also carried out by comparing the observed data with theoretical simulation for various tilt angles, indicating that the molecules are in an almost perfect flat-on orientation. Furthermore, we observed a work-function change of about -0.3 eV at the TTC/Cu(100) interface. Such a work-function change has been reported for several organic/metal systems,[45–49] and indicates the formation of a dipole layer at the interfaces in contrast to the traditional picture of energy-level alignment assuming a common vacuum level at the organic/metal interface.

II. EXPERIMENT

ARUPS measurements were carried out at the beam line 8*B*2 of the UVSOR facility at Institute for Molecular Science. The synchrotron radiation from the storage ring was monochromatized by a plane grating monochromator,[50] which can be used in the photon energy region of 2–150 eV. The ARUPS system consists of a measurement chamber, sample-cleaning chamber, and two preparation chambers.[51] The sample-cleaning chamber is equipped with a LEED/Auger optics (ULVAC-PHI RVL-120), an infrared heating system (Thermo Riko, GVH198), and an ion sputter gun (ULVAC-PHI USG-3). The base pressures of these chambers are 5×10^{-10}, 2×10^{-10}, and 1×10^{-9} Torr, respectively. The energy of the photoelectron was analyzed by a concentric electrostatic hemispherical analyzer with an angular resolution of about 3° and an overall energy resolution of about 0.2 eV at $h\nu=40$ eV, as estimated from the Fermi edge of gold. The experimental parameters such as photon incidence angle α, electron take-off angle θ, and sample azimuthal angle ϕ are defined in Fig. 2.

The Cu(100) crystal (purity of 5N) was purchased from Material-Technologie & Kristalle GmbH (MaTecK) and cleaned by repeated cycle of annealing up to about 870 K and Ar^+ ion sputtering (a primary electron-beam energy of 3 keV, a current density of 10–15 $\mu A/cm^2$, and an argon pressure of 5×10^{-5} Torr). Carbon and sulfur were main contaminants, and their concentrations at the surface were less than 5% after cleaning treatment, as judged from the measured Auger electron spectra. The LEED pattern after cleaning treatment was also characteristic of a clean, well-ordered Cu(100) surface.

The sample of TTC was purchased from Tokyo Kasei Kogyo Co. Ltd., and purified by recrystallization from benzene solution. Sample thin film was prepared by vacuum

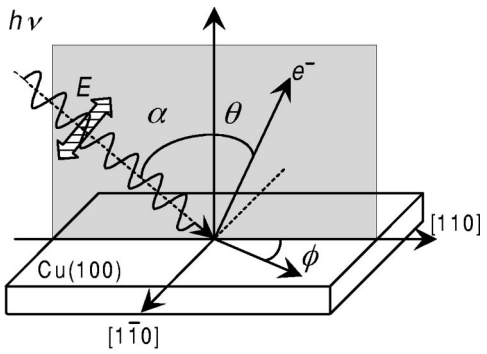

FIG. 2. Definition of the experimental parameters: the photon incidence angle, electron take-off angle, and sample azimuthal angle are denoted by α, θ, and ϕ, respectively. Incident photon beam and energy analyzer are in the same shadowed plane. This plane is perpendicular to the substrate surface and contains [110] direction of Cu(100).

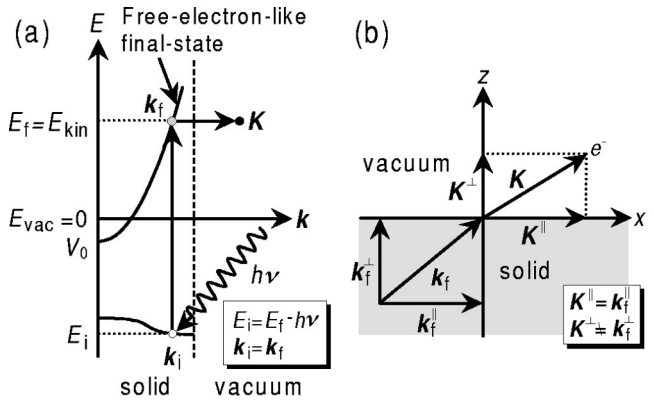

FIG. 3. Conservation of wave vector at photoemission process. (a) Photoexcitation: the wave vector of initial state $\mathbf{k}_i$ is conserved for photoexcitation, i.e., $\mathbf{k}_f=\mathbf{k}_i$. (b) Escape from the surface: the component of $\mathbf{k}_f$ parallel to the substrate is conserved at the solid/vacuum interface, while the vertical component $\mathbf{k}_f^\perp$ is not conserved.

evaporation on a clean Cu(100) substrate at room temperature. The evaporation was performed using a newly designed quartz cell in order to reduce the outgas from heater element.[52] The pressure during the evaporation was less than 2×10^{-9} Torr. The amount of deposited TTC was monitored by a quartz oscillator. Assuming that the molecular sticking coefficient on the substrate was similar to that of the quartz oscillator monitor and the density of TTC was 0.96 g/cm^3,[53] the thickness of the TTC film was estimated to be about 0.33 nm. The deposition rate was about 0.1 nm/min.

The incident photon energy $h\nu$ was 40 eV for all the ARUPS measurements. The origin of the azimuthal angle $\phi=0°$ was defined so that the electric-field vector E of the incident photon is in the plane containing the [110] direction and the surface normal (see Fig. 2). Prolonged illumination of TTC with intense light caused a change of the spectra, which is probably due to radiation damage.[54,55] In order to avoid this, the sample current was kept less than 1.2×10^{-10} A. Furthermore, the spectra were recorded with frequent changes of the sampling position on the specimen surface. The absence of damage in these cases were confirmed by remeasuring spectra for fixed combination of $h\nu$, α, θ, and ϕ after several runs.

The LEED measurements on the TTC film were performed at an incident electron energy of 130 eV, and the incident electron beam current was carefully reduced to about 2×10^{-7} A to avoid radiation damage. The LEED patterns were recorded by a conventional camera using a film of high sensitivity (ASA800). Since serious changes in the LEED pattern were observed owing to the radiation damage of the films even with such reduced current (the pattern disappeared within a few tens of seconds), the LEED measurements were carried out only after the ARUPS measurements.

III. ANALYZING METHODS OF ARUPS DATA FOR DETERMINING ENERGY-BAND DISPERSION $E=E(\mathbf{k})$

In this section, we briefly describe the method of energy-band mapping by using ARUPS data in photon energy $h\nu$ scanning mode [mode (a)] and take-off angle θ scanning mode [mode (b)]. For detailed descriptions, see, e.g., Refs. 3 and 4. The photoemission process is usually expressed by a three-step (photoexcitation, transport, and emission through the surface) model, and we make some assumptions in both modes. In Fig. 3, we show the scheme of photoemission process based on these assumptions. First, both the energy and momentum are conserved at the optical transitions of electrons, and the following relations hold:

$$E_f=h\nu+E_i, \quad \mathbf{k}_f=\mathbf{k}_i+\mathbf{G}, \tag{1}$$

where E_i, E_f, $\mathbf{k}_i$, and $\mathbf{k}_f$ are the electron energy and the wave vector of electron before and after the photoexcitation in the solid, and $\mathbf{G}$ is a reciprocal-lattice vector. When E_i and E_f are defined relative to the vacuum level, E_f corresponds to the kinetic energy of the emitted electron (E_{kin}). Second, the momentum component of the emitted photoelectron parallel to the sample surface is conserved at the propagation through the surface, because of translational symmetry along the surface,

$$E_{kin}=E_f, \quad \mathbf{K}^\parallel=\mathbf{k}_f^\parallel+\mathbf{G}^\parallel, \tag{2}$$

where E_{kin} and $\mathbf{K}$ are the kinetic energy and the wave vector of the emitted free electron. The component parallel to the surface is denoted by $\parallel$.

In mode (a), we additionally assume the following relation for a free-electron-like final state of an excited electron with a constant inner potential in the solid V_0;

$$E_{kin}=\frac{\hbar^2\mathbf{k}_f^2}{2m^*}+V_0=\frac{\hbar^2(\mathbf{k}_f^{\parallel 2}+\mathbf{k}_f^{\perp 2})}{2m^*}+V_0, \tag{3}$$

where the component of wave vector vertical to the surface is denoted by $\perp$. m^* is the effective mass of excited electron. In this case, $\mathbf{K}^\parallel=0$, and hence $\mathbf{k}_f^\parallel=\mathbf{k}_i^\parallel=0$. Accordingly, we obtain

$$\mathbf{k}_i^\perp=\mathbf{k}_f^\perp=\frac{\sqrt{2m^*(E_f-V_0)}}{\hbar}, \quad E_i=E_{kin}-h\nu. \tag{4}$$

These relations indicate that the values of E_i and $\mathbf{k}_i^\perp$ can be determined from the measured E_{kin} and $h\nu$, provided m^*

and V_0 are known. Since $\mathbf{k}_i$ changes with the change of $h\nu$ to fulfill Eq. (1), we can probe the energy-band dispersion $E_i = E_i(\mathbf{k}_i)$ along the alkyl chain. The effective mass of the excited electron m^* is often approximated by the mass of free electron m_0 ($m^*/m_0 = 1$).

In Ref. 8, using mode (a), the value of inner potential V_0 was decided by examining the $h\nu$ dependence of the photoemission intensity of the upper C $2s$ band. The intensity shows a maximum when the photon energy matches the energy separation between the C $2s$ valence band and the nearly free-electron parabola at the Γ point. By assuming that the C $2s$ band and that the free-electron-like final state band is nearly flat around the Γ point, the intensity maximum was assigned to a large joint density of states for the transition at the Γ point. From the value of $h\nu$ at this maximum, the value of inner potential was determined as -5.5 eV. However, the results of LEET experiments on long-chain alkanes[11,12] show that this assumption does not hold at low-energy region ($E_{kin} < 15$ eV). Therefore, we need to discuss the validity of this assumption.

On the other hand, in the case of mode (B), $\mathbf{K}^{\parallel}$ and $\mathbf{k}_f^{\parallel}$ are expressed as

$$\mathbf{K}^{\parallel} = \mathbf{k}_f^{\parallel} = \frac{\sqrt{2m_0 E_{kin}}}{\hbar} \sin\theta. \tag{5}$$

When the sample molecules are oriented uniaxially parallel to the substrate surface, the θ scan in a plane containing the molecular axis and the surface normal corresponds to the scan of $\mathbf{K}^{\parallel}$. Such a scan directly gives the wave vector parallel to the sample and the binding energies of the peaks in the spectra, reflecting the band dispersion in the Brillouin zone. In this case, measurements at fixed photon energy are sufficient.

Next, we will estimate the experimental resolution of wave number $\Delta\mathbf{K}^{\parallel}$. The value of $\Delta\mathbf{K}^{\parallel}$ can be obtained by differentiating Eq. (5) as

$$\Delta\mathbf{K}^{\parallel} = \Delta\left(\frac{\sqrt{2m_0 E_{kin}}}{\hbar}\sin\theta\right) = \frac{\sqrt{m_0}}{\hbar}\left(\frac{\Delta E_{kin}}{\sqrt{2E_{kin}}}\sin\theta + \sqrt{2E_{kin}}\cos\theta\,\Delta\theta\right). \tag{6}$$

For the present experiment, the values $\Delta\theta$ and ΔE_{kin} are 3.2° and 0.2 eV, respectively, as described in Sec. II. Consequently, $\Delta\mathbf{K}^{\parallel}$ is largest at the Γ point of the topmost band ($E_{kin} = 30$ eV and $\theta = 0°$), and estimated to be less than 1.6 nm^{-1}. This value is equivalent to about 7% of the Brillouin-zone (BZ) width. In addition, we have to consider some initial-state broadening of $\mathbf{k}$ (or relaxation of the $\mathbf{k}$-conservation rule) due to the small number of repeating units as reported for the system of end-on-oriented 6P on Ag.[40] Following the method in Ref. 40, the estimated size of this broadening is 0.5 nm^{-1} for the topmost band of TTC at the Γ point. It is a fair amount smaller than $\Delta\mathbf{K}^{\parallel}$, and corresponds to only 2% of the BZ width. We also consider that the lower limit of $\Delta\mathbf{k}$, given by the uncertainty principle ($\Delta x \Delta p \sim \hbar$, i.e., $\Delta\mathbf{k} \sim 1/\Delta x$), is 0.2 nm^{-1} for TTC ($\Delta x = 5.8$ nm), and the obtained $\Delta\mathbf{k}$ is very similar to this limit. This indicates that the TTC molecule has a sufficient number of repeating units for investigating the band structure.

IV. THEORETICAL SIMULATION OF ARUPS SPECTRA BASED ON THE IAC/MO APPROXIMATION

Here we explain the IAC approximation combined with *ab initio* linear combination of atomic orbitals MO calculation (IAC/MO) for the simulation of the photoelectron angular distribution. In this approximation, the photoelectron wave function is approximated by a coherent sum of the waves emitted independently from atomic orbitals which build up the molecular orbital, where the contribution of the waves scattered by the surrounding atoms is neglected. This approximation was originally proposed by Grobman,[31] and we have recently extended it to large organic molecules. The theoretical formulas of IAC/MO approximation for an organic molecule were described in the previous papers,[31–41,43,44] and we will not repeat them in detail. Briefly, the photoelectron intensity $I_n(\mathbf{R})$ from the nth MO at the detector position $\mathbf{R}$, which is far from the sample, is represented by

$$I_n(\mathbf{R}) \propto |A_{tot}^n(\mathbf{R})|^2, \tag{7}$$

where A_{tot}^n is the total amplitude of the photoelectron wave emitted from the nth MO. It is expressed as

$$A_{tot}^n(\mathbf{R}) = \sum_a \sum_{Xa} D_a C_{Xa}^n e^{-i\mathbf{k}_n\mathbf{R}_a} \sum_L Y_L^*(\hat{\mathbf{R}}) M_{LXa}, \tag{8}$$

$$M_{LXa}(k_n) = -(-i)^l e^{i\delta_l^a} \rho_l^a(k_n) \int Y_L(\hat{\mathbf{r}})\hat{\boldsymbol{\epsilon}}\cdot\hat{\mathbf{r}} Y_{Xa}(\hat{\mathbf{r}})\, d\hat{\mathbf{r}}, \tag{9}$$

$$\rho_l^a(k_n) = \int R_l(k_n r) f_{la}(r) r^3\, dr, \tag{10}$$

$$Y_{Xa}(\hat{\mathbf{r}}) = \sum_{m_a} n(m_a) Y_{La}(\hat{\mathbf{r}}), \tag{11}$$

where D_a is the phenomenological damping factor for the photoelectron wave along $\mathbf{R}$ from atom a to the surface corresponding to inelastic process. C_{Xa}^n is the nth molecular orbital coefficient of the Slater-type atomic orbital Xa ($= s, p_x, p_y, p_z$), and $\mathbf{R}_a$ is the position of the atom a. k_n ($= k_n\hat{\mathbf{R}}$) is the photoelectron wave vector, $\hat{\mathbf{R}}$ is the direction of detector, and the origin of $\mathbf{r}(= r\hat{\mathbf{r}})$ is put on the center of each atom. The angular momenta of the initial and final states are denoted by $L_a = (l_a, m_a)$ and $L = (l, m)$, respectively. The transition matrix element M_{LXa} which includes the phase shift δ_l^a and the radial integral $\rho_l^a(k_n)$ can be described as Eq. (9). The value of δ_l^a and the radial part of the final wave function $R_l(k_n r)$ were calculated in muffin-tin potentials[56] with use of the atomic wave functions calculated by Harman and Skillman.[57] $f_{la}(r)$ is the radial part of the initial atomic wave function. $Y_{Xa}(\hat{\mathbf{r}})$ is the spherical part of the atomic orbital Xa, which is described as the linear combination of spherical harmonics $Y_{la}(\hat{\mathbf{r}})$. Thus Eq. (8) repre-

sents the self-scattering wave emanating from each atomic site, where the summation with a is carried out over all atoms in a molecule.

In the present calculation, we employed the *ab initio* MO calculations with the Hartree-Fock method in order to obtain the values of C_{Xa}^{n} and eigenvalue for each MO. The calculations were performed with minimal basis set using the program generalized self-consistent field calculation 3 (GSCF3) coded by Kosugi.[58] The atomic coordinates were calculated with parameters of 0.154 nm (C—C bond), and 0.109 nm (C—H bond) for the bond lengths, and a tetrahedral angle 109.28° for the bond angle, respectively. The axes were taken so that the x and y axes in the C—C—C plane, with the x-axis parallel to the alkyl-chain axis. Due to the capacity limitation of the program for IAC calculation, we performed this calculation for a dotriacontane (n-$C_{32}H_{66}$; DTC) molecule. This choice does not cause a problem in interpreting the observed data of TTC, because the electronic structure of long-chain alkane is known to be almost independent of the carbon number n at about $n \geq 10$,[59,60] and the size of blurring effect in $\Delta\mathbf{k}$ mentioned in Sec. III is estimated to be $0.6\,\mathrm{nm}^{-1}$ for DTC, which is almost the same with that for TTC ($0.5\,\mathrm{nm}^{-1}$). The values of the phase shift and radial integral for C $2p$, C $2s$, and H $1s$ were calculated by assuming a muffin-tin radius of 0.1 nm in order to avoid the deformation of the potential at low kinetic-energy region of emitted photoelectrons.

V. RESULTS AND DISCUSSION

A. Analysis of LEED pattern

In Fig. 4(a) we show a typical LEED pattern of a TTC thin film (0.33 nm thick) on the Cu(100) substrate, where the LEED patterns from the substrate and the TTC film coexist. Figure 4(b) shows the schematic view of the LEED pattern of TTC/Cu(100) and the assignments of the spots. The diffraction spots from the Cu(100) substrate and from the TTC film correspond to the circles and crosses, respectively. Considering the symmetry of the substrate lattice, the obtained LEED pattern can be interpreted as the overlapping contributions from the two domain structures with a 2×1 lattice of TTC film against the (100) lattice of the Cu substrate.

The geometrical parameters and the definition of the axes of a TTC molecule are shown in Fig. 5. The bond lengths and bond angles of the TTC molecule are taken to be 0.154 nm (C—C bond), 0.113 nm (C—H bond), 114.6° (∠C—C—C), and 110.4° (∠H—C—H), respectively, following the data of gas-phase electron diffraction of n-hexadecane.[62] Using these parameters, the length of the repeating C_2H_4 unit along the alkyl-chain direction was calculated to be 0.259 nm, and this value is very close to the bond length of Cu atoms (0.256 nm). Assuming that the van der Waals radius of hydrogen is 0.12 nm,[63] the widths of a TTC molecule along the y and z axes in Fig. 5 are 0.45 and 0.43 nm, respectively. These values are close to twice the Cu bond length (0.512 nm). Thus we can consider that the obtained LEED pattern reflects a structure with a periodicity twice the Cu-Cu distance along the axis orthogonal to the alkyl-chain direction, and parallel to the substrate in the real space. The observation of only half-order extra spots may at

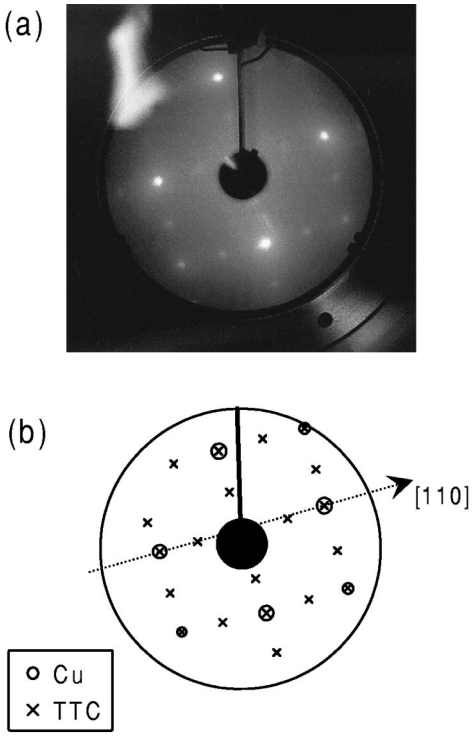

FIG. 4. (a) Observed LEED pattern of a TTC thin film (0.33 nm thick) on the Cu(100) substrate. The primary beam energy and the current are 130 eV and about 2×10^{-7} A, respectively. (b) Schematic view of the LEED pattern of TTC/Cu(100). The diffraction spots from the Cu(100) substrate and from the TTC film are indicated by circles and crosses, respectively. The dark area at the center of the view port is the electron gun, and the (0,0) spot is hidden in this region.

first sight seem to be inconsistent with the possible large unit cell of a TTC overlayer. This can be explained by the fact that the observed LEED pattern does not reflect the intermolecular periodicity along the alkyl-chain direction, but reflects the periodicity of the C_2H_4 units in the molecule, since the chain length of TTC (5.8 nm) is comparable to the co-

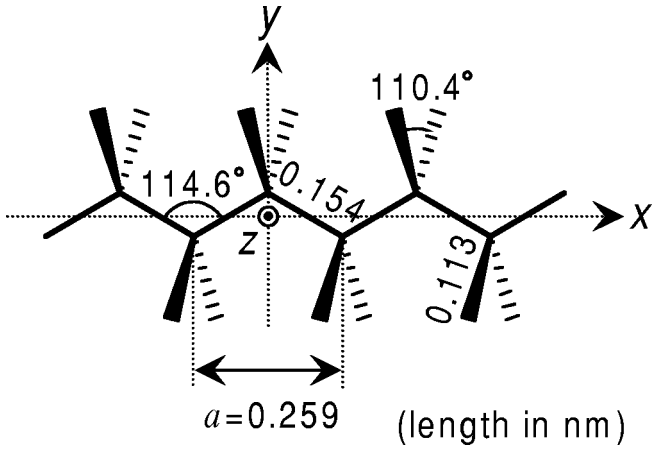

FIG. 5. Geometrical parameters and the molecular coordinate system of n-alkane. The values are taken from Ref. 62. The alkyl-chain axis is along the x axis, and the C—C—C plane of n-alkane is on the xy plane. The repeating unit length of the alkyl chain is 0.259 nm.

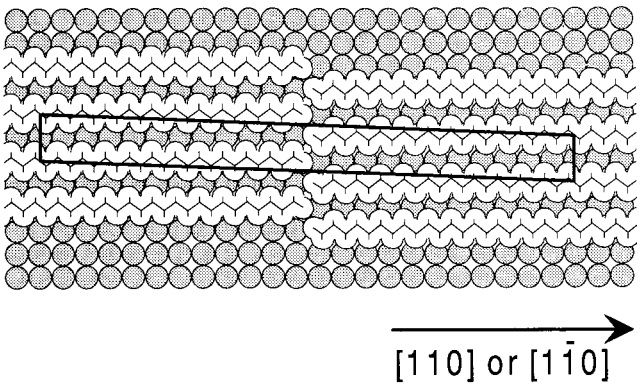

FIG. 6. A possible arrangement of TTC molecules with the unit mesh of TTC and the Cu(100) lattice in the space. In this scheme, we assume a flat-on orientation and an all-*trans* structure of the TTC molecule. The shape of the TTC molecule is indicated by solid lines corresponding to the C—C and C—H bonds, and the arcs representing the van der Waals radius (0.12 nm) of hydrogen atoms. The unit lattice is calculated to be $5.89\times0.512\ \mathrm{nm}^2$ separated by 85°.

herence width of the incident beam, which is typically 5–10 nm.[61] This interpretation indicates either the flat-on or edge-on orientation of TTC molecules with their axis of the alkyl chain (the *x* axis) along the [110] and [1$\bar{1}$0] directions of the Cu substrate. However, from the results of LEED measurements only, we cannot determine which of the flat-on or edge-on orientations is realized, because the size of the unit mesh is almost the same for these orientations.

Figure 6 shows the proposed arrangement of TTC molecule with the unit meshes of TTC ($5.89\times0.512\ \mathrm{nm}^2$ separated by 85°) and Cu(100) square lattice ($0.256\times0.256\ \mathrm{nm}^2$) in real space. In this scheme, we assume a flat-on orientation and an all-*trans* structure of the TTC molecule. The assumption of an all-*trans* structure is based on the coverage dependence of IR-RAS experiments for TTC on Ag(111), Au(111), and Cu(100).[23–25] According to these works, the structure of first layer of TTC is flat-on and contains no gauche structure. In the present work, the LEED pattern and the observed intramolecular energy-band dispersion mentioned below (Sec. V B 2) also support an all-*trans* structure. We could not deduce the detailed adsorption geometries because of the lack of information about the adsorption site. As mentioned in Sec. I, a similar parallel orientation has also been observed for short *n*-alkanes (n-C_3H_8-n-C_8H_{18}) on Ag(111)[15] and Pt(111)[16] by Firment and Somorjai, and for hexatriacontane (n-$C_{36}H_{74}$;HTC) on Cu(111)[27] by Dudde and Reihl. Furthermore, this orientation was deduced by Ito *et al.*[18] for a TTC monolayer film evaporated on polycrystalline metal (Au, Ag, and Pb) substrates.

As for the thickness of the TTC film, the area occupied by a TTC molecule is about $3.0\ \mathrm{nm}^2$ based on the above-mentioned unit mesh of the TTC film. Therefore, the weight of TTC monolayer per unit area is estimated to be $3.4\times10^{-8}\ \mathrm{g/cm}^2$. On the other hand, the weight of TTC molecules deposited on the quartz oscillator of the thickness monitor was $3.2\times10^{-8}\ \mathrm{g/cm}^2$. Consequently, the thickness of the TTC film used in this study was deduced to be equivalent to about 0.9 ML.

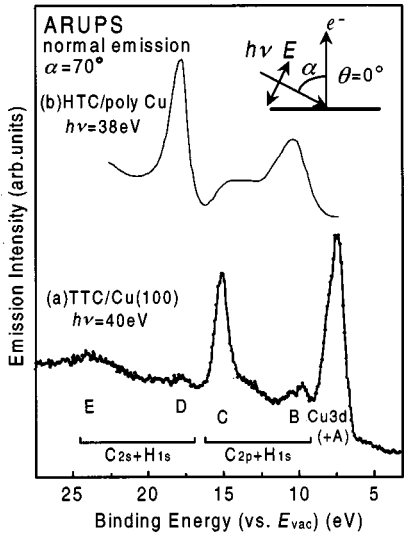

FIG. 7. (a) Normal-emission ($\theta=0°$) ARUPS spectrum of a TTC thin film on Cu(100) at $\alpha=70°$. The incident photon energy is 40 eV. (b) Normal emission spectrum of an end-on-oriented hexatriacontane (HTC) film on contaminated Cu polycrystalline plate taken from Ref. 8 under the same experimental setup as in the present study. The labels of the peaks correspond to those in Fig. 8.

B. Electronic structure and molecular orientation of TTC measured by ARUPS

1. Normal-emission spectra and molecular orientation

Figure 7(a) depicts the ARUPS spectrum of a TTC thin film on Cu(100) for normal emission ($\theta=0°$) at a photon incidence angle α of 70°. Since the alkyl chain of TTC is parallel to the substrate, the shape of the normal-emission spectrum reflects the electronic structure of TTC at the Γ point in the Brillouin zone, where the parallel component of the wave vector along the chain is zero. The abscissa is the binding energy relative to the Fermi level (E_F) of the substrate, and the spectra, are normalized to the incident photon flux. As a reference, in Fig. 7(b) we show the ARUPS spectra of the end-on oriented n-$C_{36}H_{74}$ (HTC) film[8] on a contaminated polycrystalline Cu substrate in the same experimental setup for α and θ.

As mentioned in Sec. I, long-chain *n*-alkanes are good model compounds of polyethylene, and many detailed theoretical studies of their electronic structures have already been reported.[8] In Fig. 8, the orbital assignments and shapes of the corresponding molecular orbital patterns and symmetries at the Γ point are shown.[64] Because of the thickness of the TTC film (0.33 nm) is smaller than the electron escape depth [$\simeq$2.5 nm at $h\nu=40$ eV (Ref. 65)], the 3*d* band structure of the Cu substrate is also observed in the binding energy region of 2–4.5 eV in Fig. 7(a). The uppermost state of TTC (b_{2g} symmetry at Γ) in this energy region cannot be clearly seen due to the overlap with this Cu 3*d* peak. So this peak was denoted by Cu $3d+A$. Peak *B* (9.8 eV) consists of C $2p_z$+H 1*s* bands (b_{1g} symmetry at Γ) and C $2p_y$+H 1*s* bands (a_g symmetry at Γ). Peak *C* (15.2 eV) is derived from the C $2p_z$+H 1*s* bands (b_{2u} symmetry at Γ). The $1b_{1g}$ and $1b_{2u}$ molecular orbitals, derived mainly from the C $2p_z$ orbitals, are so-called pseudo-π orbitals. Peaks *D* (18.0 eV)

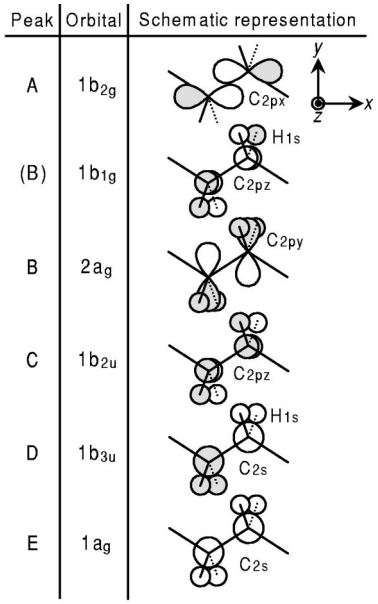

FIG. 8. Schematic representation of molecular orbitals for polyethylene and the corresponding symmetries at the Γ point.

and E (24.1 eV) are derived from C $2s$ + H $1s$ bands, with $1b_{3u}$ and $1a_g$ orbitals at Γ, respectively.

By comparing the spectra in Figs. 7(a) and 7(b), we find drastic differences in the peak intensities owing to the different molecular orientations. Since we can exclude the possibility of end-on orientation, the application of the selection rules[3] to flat-on or edge-on geometries will be discussed. Selection rules for long-chain n-alkane adsorbed on the metal substrate was reported for a HTC film on Cu(111) at an experimental geometry ($\alpha=60°$ and $\theta=0°$) similar to ours. They concluded upon edge-on orientation, but there was some error in the arguments of the selection rules. The error in Ref. 27 was already pointed out in Ref. 28, and the orientation of HTC/Cu(111) was corrected to be flat-on. Therefore, we will briefly consider the orientation of a TTC molecule on Cu(100) by following the arguments in Ref. 28.

The symmetry elements for free all-*trans* polyethylene at the Γ point is isomorphous with the factor group D_{2h}.[66–68] But this symmetry is reduced when the molecule adsorbs on the substrate owing to the existence of substrate. In Fig. 9, we show the symmetry operation for systems with parallel orientations (flat-on and edge-on). The intramolecular coordinate is defined as shown in Fig. 5. In the case of flat-on (edge-on) orientation, there are three symmetry operations, $\{C_2(z)|a/2\}$ ($\{C_2(y)|0\}$), $\{\sigma(xz)|a/2\}$ ($\{\sigma(xy)|a/2\}$), and $\{\sigma(yz)|0\}$, where a is the C_2H_4 unit cell length. In Table I, we summarize the reduced symmetry of orbitals of a parallel-oriented alkyl chain at the Γ point by considering the existence of a substrate.

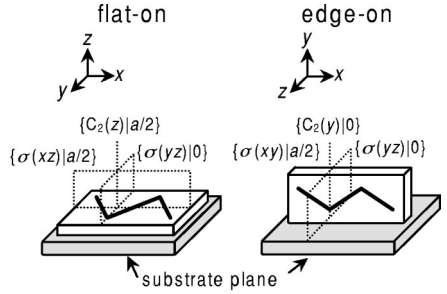

FIG. 9. Symmetry operations for parallel orientations. The coordinate is defined as shown in Fig. 5, and fixed to the molecule. We assumed the perfect polarization of the electric vector of incident light along the surface normal.

In the experimental setup of the present study, the electric vector of the light can be regarded as almost polarized along the surface normal. Thus the representation of the electric vector belongs to A_1. In order to detect photoelectrons at normal emission, the final state should be symmetric with respect to the all-symmetry operations along the surface normal. Therefore, the transition-allowed initial states are the orbitals with a_1 symmetry in Table I. Consequently, the $1b_{2u}$ orbital (peak C), which appears as a strong peak in Fig. 7(a), can be allowed only for the flat-on orientation. When we look at other peaks in Fig. 7(a), peaks B and E are clearly seen, while peak D is very weak. These are also consistent with the expected trends in Table I for flat-on orientation. We can also observe the weak emission of peak D in Fig. 7(a), which is forbidden state for flat-on orientation. This is probably because of the disorder of the film and the imperfect polarization of the incident light. In this way, we could determine the surface orientation of TTC on Cu(100) by selection rules, and conclude that the orientation of TTC on Cu(100) is flat-on, as in the case of other n-alkanes deposited on Cu(111) surface.

2. Take-off angle dependence of the ARUPS spectra

In Fig. 10, we show the dependence of the ARUPS spectra on the take-off angle θ for a thin film of TTC on Cu(100)

TABLE I. Summary of the reduced orbital symmetry for parallel orientations, peak assignments, and orbital charactors at the Γ point. The allowed and forbidden transition states are denoted by ○ and ×, respectively.

Orbital	Reduced symmetry (C_{2v})		Peak assignments	Orbital
symmetry in D_{2h}	flat-on	edge-on	in Fig. 7(a)	charactors
$1b_{2g}$	a_2(×)	b_1(×)	A (hidden)	C $2p_x$ + H $1s$
$1b_{1g}$	b_2(×)	b_2(×)	(B)	C $2p_z$ + H $1s$(pseudo-π)
$2a_g$	a_1(○)	a_1(○)	B	C $2p_y$ + H $1s$
$1b_{2u}$	a_1(○)	b_2(×)	C	C $2p_z$ + H $1s$ (pseudo-π)
$1b_{3u}$	b_2(×)	a_1(○)	D	C $2s$ + H $1s$
$1a_g$	a_1(○)	a_1(○)	E	C $2s$ + H $1s$

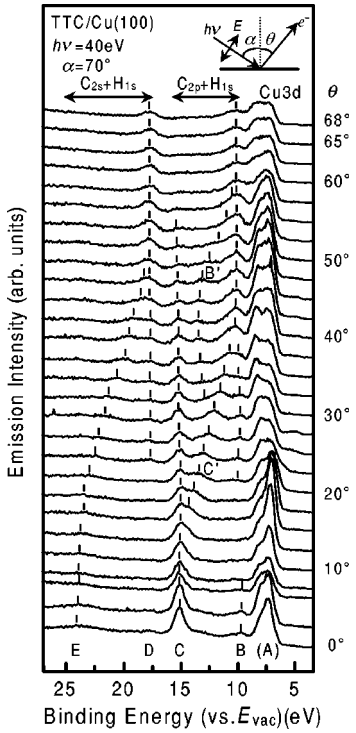

FIG. 10. Take-off angle θ dependence of the ARUPS spectra for an ultrathin film of TTC on Cu(100). The abscissa is the binding energy relative to the vacuum level (E_{vac}). The photon incidence angle α is 70°, and θ is varied from 0° (normal emission) to 68°. The labels of the peaks correspond to those in Figs. 7 and 8.

normalized by the photon intensity. The abscissa is the binding energy relative to the vacuum level (E_{vac}). The photon incidence angle α is 70°, and θ is varied from 0° (normal emission) to 65°, with a steps of 2.5°. Variations in both the position and intensity of the spectral features can be clearly observed. As mentioned in Sec. V B 1, peaks *B* and *C* are derived from the C $2p+$H $1s$ bands. When we start from $\theta=0°$ at the bottom, the position of peak *B* is fixed, but its intensity changes with θ, with a maximum at $40° \leqslant \theta \leqslant 50°$. Peak *C* also has a fixed peak position, and its intensity decreases with increasing θ. With the increase of θ, two new features labeled B' and C' appear in the region between peaks *B* and *C*. Peak B' appears at $\theta=27.5°$, and shifts in the range between 5.5 and 8.5 eV. Peak C' appears near peak *C* at $\theta=12.5°$, and merges into peak *B* after a gradual shift. Peaks *D* and *E*, which originate from the C $2s+$H $1s$ bands, have a weaker intensity than the peaks originating from the C $2p+$H $1s$ bands. Peak *D* shows no shift in the peak position, but its intensity increases with increasing θ. Peak *E* shows a large shift towards lower binding energy with increasing θ, and merges into peak *D* at $\theta=50°$. Since the LEED patterns and the results of normal-emission spectra indicate the parallel orientation to the surface, we can expect that parallel component of wave vector is a good quantum number in the off-normal spectra, and that the observed behaviors reflect the intramolecular energy-band dispersion in a TTC molecule. In Sec. V B 3, we deduce the dispersion and compare the results with the reported band calculations for polyethylene.

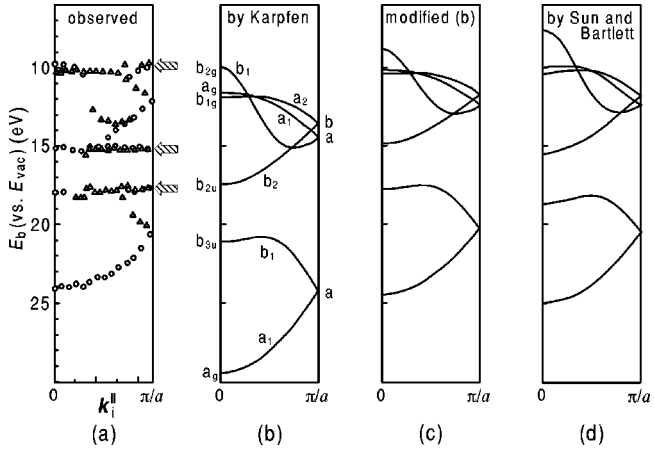

FIG. 11. (a) Experimentally obtained one-dimensional intramolecular energy-band structure plotted in the reduced zone scheme. The abscissa is the parallel component of the wave vector $\mathbf{k}_i^{\parallel}$ along the [110] direction of the Cu(100) substrate. The Brillouin-zone (BZ) boundary ($\mathbf{k}_i^{\parallel}=\pi/a$) is at 0.121 nm^{-1}. (b) and (c) Calculated band structure for all-*trans* polyethylene from Ref. 69. The band in the original energy scale and in a modified scale (contracted 0.8 times and shifted) are shown in (b) and (c), respectively. (d) Calculated band structure for all-*trans* polyethylene from Ref. 71 in which the value of **k** was modified from the original one (see text).

3. Intramolecular one-dimensional energy-band dispersion of TTC

The experimentally obtained one-dimensional intramolecular energy-band structures is plotted in a reduced zone scheme in Fig. 11(a). The abscissa is the parallel component of the wave vector $\mathbf{k}_i^{\parallel}=\mathbf{K}^{\parallel}$ along the [110] direction of the Cu(100) substrate. The value of $\mathbf{k}_i^{\parallel}$ is calculated by using Eq. (5). We used lengths of repeating units of alkyl chains *a* of 0.259 nm. This leads to a width of the BZ boundary ($\mathbf{k}_i^{\parallel}=\pi/a$) of 0.121 nm^{-1}. By scanning θ in the range of 0°–68°, we can cover the whole BZ. In Fig. 11(a), the circle and triangle indicate the data points in the first and second BZ's, respectively. Figure 11(b) shows the result of a Hartree-Fock-type *ab initio* band-structure calculation by Karpfen for an all-*trans* polyethylene chain.[69] Comparing Figs. 11(a) and Fig. 11(b), there are large discrepancies in the energy scale; in particular, the discrepancies become larger at high binding energy. Figure 11(c) is the band structure in Fig. 11(b), which is contracted 0.8 times and shifted in the energy scale for better correspondence with the experimentally obtained one. This modification was also applied to compare the calculation with the experimental result in Refs. 5–10.

The discrepancy in energy scale is an essential problem of a Hartree-Fock-type theoretical calculation. By assuming Koopmans' theorem with a frozen orbital approximation, the ionization potentials are obtained by inverting the sign of the eigenvalues of the Hartree-Fock ground-state orbital. But the effects of the relaxation of the orbital and the electron correlation are neglected. Consequently, the reliability of this type of calculation on the energy scale is rather low. Recently, some theoretical trials for improving this problem have been reported. Deleuze and Cederbaum made simulations of the x-ray photoemission spectroscopy (XPS) spectra

of saturated hydrocarbons by means of a one-particle Green's-function calculation,[70] and Sun and Bartlett calculated the band structures of all-*trans* polyethylene, in addition to the simulation of XPS spectrum based on the many-body perturbation theory for finite system.[71] In both these studies, better correspondence in the energy scale was achieved. Figure 11(d) shows the calculated band structures of Ref. 71 in the reduced zone scheme. There might be some mistake in calculating **k** in Ref. 71, so we regarded the full scale of **k** in the calculation as the first and second BZ's with the assumption of a repeating unit of the polyethylene taken to be C_2H_4. The band structures in Fig. 11(d) show excellent correspondence with the one of Fig. 11(a), without any contraction factor or energy shift. But there are still some differences from the experimentally obtained features in the ranges of 12.5–14 and 24–25 eV. There is also some discrepancy between the calculations in (c) and (d) about the top part of the occupied state.

The correspondence between the observed and calculated band structure indicates that well-oriented TTC films with their long chain axes parallel to the surface were actually prepared. However, we also see additional features with constant energies indicated by hatched arrows in Fig. 11(a). We attribute this to the two-domain structure of the TTC film. That is, the measured spectra consist of components of $\phi = 0°$ and 90°, with the alkyl-chain axes parallel and vertical to the plane which contains the electric-field vector and energy analyzer (see Fig. 2), owing to the symmetry of the substrate. The energy positions of the features in the spectra for $\phi = 90°$ exhibit no dispersion, because the component of wave vector along the alkyl chain is always zero.

Next we compare the experimentally obtained band structures with those of Ref. 8. The general features of these band structures are very similar. But in the band structure of Ref. 8 which is obtained with mode (a), the data points for the bottom of pseudo-π band (around 15 eV in binding energy and mainly consisting of C $2p_z$ and H 1s orbitals; see Fig. 8) are much scattered than for other bands. Considering the selection rules of mode (a) with the electric vector polarized along the surface normal, the pseudo-π band should be forbidden because this band is always antisymmetric with respect to the C—C—C plane. Actually, the emission intensity of this state in Fig. 7(b) is much weaker than the transition-allowed peaks. Such a small intensity will cause the ambiguity of the energy of the lower part of the pseudo-π band.

On the other hand, in this work, the lower part of the pseudo-π band is allowed in all areas of the BZ, and we can map the lower part of the pseudo-π band more precisely with mode (b). However, the upper part of the pseudo-π and C $2s$ bands should be forbidden in mode (b). These results indicate that these complementary measurements with modes (a) and (b) are important for investigating the complete band structure of long-chain alkanes.

To end this section, we mention the validity of the assumption of a free-electron-like final state, and the estimation of the inner potential V_0 in Refs. 5–10. As mentioned in Sec. III, the estimation of the inner potential was based on the emission intensity of the C $2s$ band, which is allowed transition in mode (a). Judging from the similarity of the obtained band diagram with the present one, we can consider that the final state can actually be assumed to have free-electron-like parabola with the approximation of $m^*/m_0 = 1$, and the estimated value of V_0 in these reports was a good estimation for the band mapping.

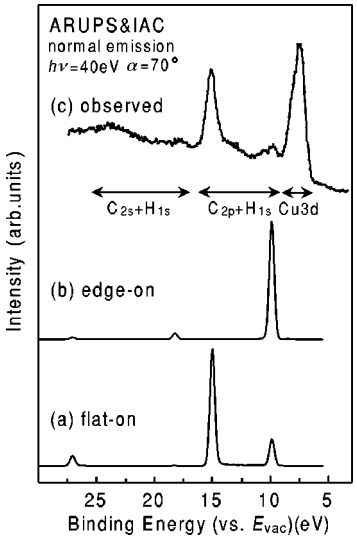

FIG. 12. (a) and (b) Simulated spectra by the IAC/MO approximation for the flat-on and edge-on orientations, respectively. The calculations were performed under the conditions of $\alpha = 70°$, $\theta = 0°$, and $h\nu = 40$ eV. These spectra were obtained by the convolution with a Gaussian function (the FWHM is 0.5 eV), and are normalized by the maximum height of the peak. The emission from two types of orientations with alkyl-chain axes along the [110] ($\phi = 0°$) and $[1\bar{1}0]$ ($\phi = 90°$) directions are summed up. (c) The observed spectrum for normal emission shown in Fig. 7(a).

C. Simulation of ARUPS spectra with IAC/MO approximation

1. Comparison of simulated and observed spectra for normal emission

We start the simulation with the IAC/MO approximation from those for typical flat-on and edge-on orientations. We can omit the possibility of end-on orientation as described in the previous sections. The simulated spectra are shown in Figs. 12(a) and 12(b). In this work, the effect of the molecular vibration is neglected, and the simulated UPS spectra were obtained simply by the convolution of δ functions at orbital energies with a Gaussian function [the full width at half maximum (FWHM) is 0.5 eV]. The calculation was performed for a DTC molecule under the same condition with the experimental setup ($\alpha = 70°$, $\theta = 0°$, and $h\nu = 40$ eV) assuming a perfect polarization of synchrotron radiation in the horizontal plane. The abscissa is the calculated binding energy relative to the vacuum level (E_{vac}). As mentioned in Sec. V B, experimentally observed spectra of TTC/Cu(100) are the sum of the emission from TTC molecules oriented with their long-chain axes along the [110] direction ($\phi = 0°$) and the $[1\bar{1}0]$ direction ($\phi = 90°$), reflecting the fourfold symmetry of the substrate. Thus we calculated the emission intensity from these two orientations and added them with equivalent weights. The shapes in the 13–20 and 23–32 eV regions in binding energy correspond to the emission from the states derived from the C $2p+$H $1s$ and C $2s$

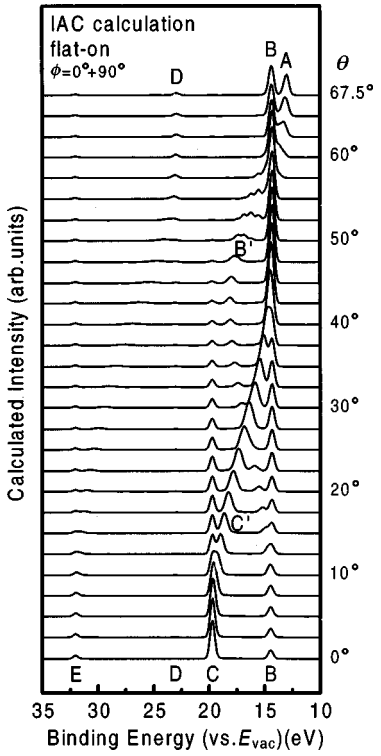

FIG. 13. Take-off angle θ dependence of the simulated spectra for the flat-on orientated dotriacontane (DTC) molecule calculated by the IAC/MO approximation. The calculation is performed under the condition of $h\nu=40$ eV, $\alpha=70°$, and $\theta=0°-67.5°$. Each simulated spectrum is the sum of the spectra for $\phi=0°$ and 90°.

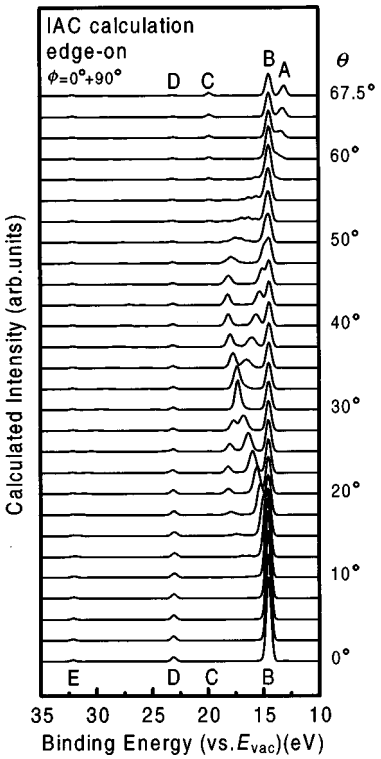

FIG. 14. Take-off angle θ dependence of the simulated spectra for the edge-on orientation. The calculation is performed under the same condition as those for Fig. 13.

+H 1*s*, respectively. Figure 12(c) shows the observed spectra for normal emission, which was already shown in Fig. 7(a), and this curve is shifted toward higher binding energy to fit the position of peaks *B* and *C* with the simulated spectra. At higher binding energy, there is a large discrepancy in peak position. This is because we performed the MO calculation with the Hartree-Fock level, as mentioned in Sec. V B 3. The relative intensity of the simulated spectra for the flat-on orientation shows good agreement with the observed spectra. This confirms our results of the selection rules.

2. Take-off angle dependence of the simulated spectra for parallel orientations

In Fig. 13, we show the take-off angle θ dependence of the simulated spectra for a DTC molecule with a flat-on orientation. The photon incidence angle is 70°, and the take-off angle θ is varied from 0° to 67.5° with steps of 2.5°. The abscissa is the binding energy relative to E_{vac}. The emission intensities for azimuthal angles of $\phi=0°$ and 90° are summed up. Behaviors of the peak positions and intensities in the simulated spectra for flat-on orientation are in excellent agreement with the observed spectra. For example, the behavior of the peak intensities of *C* and *D*, and the peak shifts of *B'*, *C'*, and *E* in Fig. 10 are well reproduced. The simulated spectra, assuming an edge-on orientation, are also shown in Fig. 14. Comparing these spectra with the observed ones, we can see clear differences among them. In particular, the intensities of peaks *C* and *D* of the observed spectra show behavior that is completely reversed compared to the calculated one.

Figure 15 shows the energy-band dispersion obtained from the simulated spectra for flat-on orientation. The data points derived from the spectra for $\phi=0°$ and 90° are represented by open and filled circles, respectively. This band-diagram confirms our assignment of the additional features indicated by the arrow in Fig. 11(a) to the contribution from the molecules with $\phi=90°$.

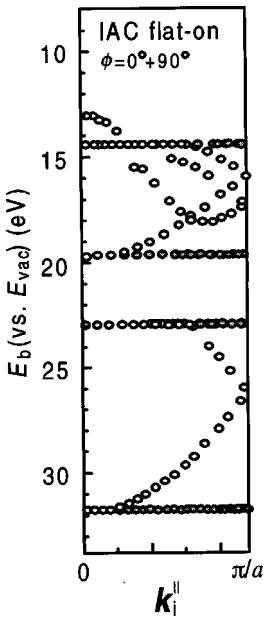

FIG. 15. Energy-band structure obtained from the simulated spectra for the flat-on orientation. The data points derived from the spectra for $\phi=0°$ and 90° are represented by filled and open circles, respectively.

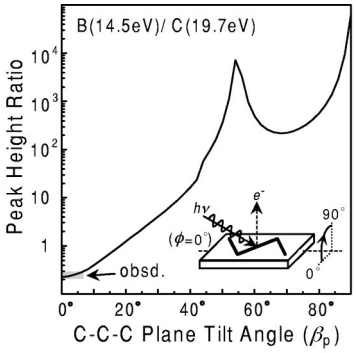

FIG. 16. The ratio between the intensities at the fixed energy position of 14.5 eV (peak B) and 19.7 eV (peak C) against the tilt angle of the C—C—C plane at the Γ point for $\alpha=70°$, and $\theta=0°$. The tilt angle of the C—C—C plane is varied 0° to 90°, with a step of 2°.

Thus the results obtained by simulated spectra confirm the flat-on orientation of TTC films on a Cu(100) surface, and also demonstrate the validity of the IAC/MO calculation for saturated compounds. Therefore, the reliability and usefulness of a theoretical simulation with the IAC/MO approximation was confirmed not only in the case of π-conjugated systems but in the case of a σ-electron system.

3. Analysis of the tilt angle of the C—C—C plane and the alkyl-chain axes of TTC

So far we have examined the molecular orientation only in terms of a choice among the three typical orientations shown in Fig. 1. Now we will examine whether the molecules are exactly in the flat-on orientation by comparing the observed spectrum at normal emission with calculations at various tilt angles of the C—C—C plane and the chain axes of TTC. Such a quantitative examination was not possible by a discussion based on the selection rules.

We focus our attention on the intensity ratio of peak B to peak C at the Γ point since (i) peak Cu $3d+A$ obviously can not be compared with calculated spectra, and (ii) the intensities of peaks D and E are difficult to estimate due to the weak contrast in the background. In Fig. 16, the calculated ratio of peak B to C is plotted against the tilt angle of C—C—C plane β_p. The calculation was performed for $\alpha=70°$ and $\theta=0°$, by changing β_p in the region of 0°–90° with steps of 2°. The peak height at the fixed energy position of 14.5 and 19.7 eV were used as the intensity of peaks B and C, respectively. The contributions from the orientations with $\phi=0°$ and 90° were summed up for the calculation of the peak intensities. The obtained results show a very large change, as seen in the use of logarithmic scale in the ordinate. The observed B/C ratio is 0.2–0.3, corresponding to a β_p of 0°–7°. This result indicates that the C—C—C plane is almost perfectly parallel to the substrate surface.

As for the tilt angle of alkyl-chain axis, we also performed simulation for normal-emission spectra. Figure 17(a) shows the simulated spectra for various values of the tilt angle β_a of the chain axis in the region of 0°–18° with steps of 2°. These spectra are obtained by the convolution of a Gaussian function with a FWHM of 0.5 eV. Different from the case of the tilting of the C—C—C plane, the dispersion

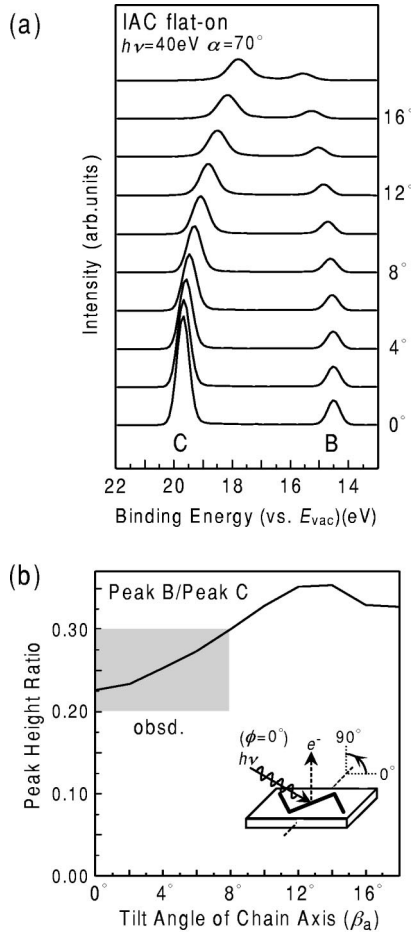

FIG. 17. (a) Simulated spectra for various values of the tilt angle of chain axis in the region of 0°–18° with a steps of 2°. The FWHM of these spectra is 0.5 eV. (b) Calculated ratio of the intensity between peaks B and C in the region of 0°–18°.

of peaks B and C occurs as the tilt angle β_a changes. This is because the change of β_a causes the change of wave vector along the chain direction. Therefore, the bottom of the pseudo-π band can be probed for normal emission only when $\beta_a=0°$. Figure 17(b) shows the calculated ratio of the intensity between peaks B and C in the region of 0°–18°. The contributions from orientations with $\phi=0°$ and 90° were summed up for the calculation of the peak intensities. In this figure, the experimentally obtained B/C ratio of 0.2–0.3 corresponds to a tilt angle less than 8°. Since the variation of the B/C ratio with β_a is rather small, one may suppose that this estimation of β_a is not definite. However, in additional measurements (not shown) we observed that the position of the pseudo-π band is shifted back toward the low-binding-energy side as θ is changed to the negative side. This implies that the bottom of the pseudo-π band at the Γ point is actually reached around normal emission ($\theta=0°$), indicating that $\beta_a\simeq 0°$. Thus it is reasonable to conclude a parallel orientation of the alkyl chain to the substrate surface with a tilt angle of $\leqslant 10°$.

We should admit that the accuracy of this estimation is not very high, since the overlap of the emission from the substrate and the calculated intensities may also contain some errors due to the ambiguity in parameters such as the

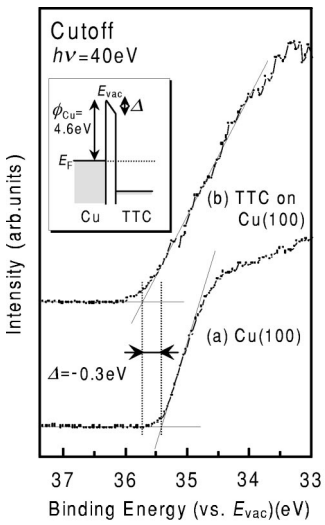

FIG. 18. Low-kinetic-energy region of spectra before (a) and after (b) the deposition of TTC. The incident photon energy is 40 eV, with an incident angle of light $\alpha = 50°$, and photoelectrons emitted to the surface normal ($\theta = 0°$) were detected. Inset: energy diagram for the TTC/Cu(100) interface.

molecular geometry, the neglect of the scattering effect, and the assumption of a perfect polarization of the incident light. However, we can still say that the calculation reproduced the experimental data reasonably well. This indicates that the molecular orientation of TTC on Cu(100) can be regarded as nearly exact flat-on orientation.

D. Work-function change at TTC/Cu(100) interface

Finally, we wish to report additional information about interfacial electronic structure. Recently, the applications of functional organic compounds to the electric devices such as photovoltaic cell and electroluminescent devices have attracted much interest.[72] The study of the electronic structure of the organic/metal interface is indispensable for an understanding of the mechanisms of such devices. In most studies on organic devices, the interfacial electronic structure has been estimated with the traditional model of energy-level alignment, assuming a common vacuum level at the organic/metal interface. We have indicated in previous reports[18,45–49] that the traditional model is not valid, and the work-function change Δ exists at the interface. This means that the interfacial dipole layer is formed at the interface. In order to obtain more detailed information about the origin of Δ, an investigation of a well-ordered organic thin film on a well-defined metal surface is needed. Therefore, the TTC/Cu(100) system in this study has an important meaning as the model of such an organic/metal interface.

We measured the work-function change at the deposition of TTC on a Cu(100) surface from the low-energy cutoff of the spectra. Figures 18(a) and 18(b) show the low-energy cutoff of the Cu(100) substrate before and after evaporation. The incident phtoton energy was 40 eV, and the incident angle was 50°. Photoelectrons emitted normal to the surface were detected. During the measurement of low-energy cutoff, the sample was biased -5 eV for ensuring that the cutoff is not determined by the work function of the energy analyzer. The abcissa is the binding energy from the vacuum level. From these data, the work function of the Cu(100) surface is calculated to be 4.6 eV based on Eqs. (1) and (2). The energy position difference of the cutoff, that is, the work-function change Δ by the adsorption of TTC, is estimated to be about -0.3 eV.

A similar work-function change has been observed for TTC/evaporated metals[18] and TTC/Au(111)[49] systems. As for the origin of Δ, we discussed several models in Refs. 49 and 75. In the present case, the adsorption of TTC on Cu(100) can be regarded as physisorption, because the heat of adsorption for short alkanes on Cu(100) and Pt(111) reported by Sexton and Hughes[73] is very small. Therefore, the origin of Δ is owing to some physical effects. We can point out the following two effects as the possible origin. One is the image effect[74] which is the explanation for the Xe/metal system. The other one is the surface rearrangement of an electron cloud of metal spilled out to the vaccum induced by the adsorption of a molecule. For a complete understanding of the origin of Δ, we require further discussion with the aid of some theoretical treatment.

VI. SUMMARY

The electronic structure and molecular orientation of a tetratetracontane (TTC) ultrathin film on Cu(100) were studied by ARUPS measurements using synchrotron radiation with the aid of theoretical calculations in an IAC/MO framework. By analyzing the LEED pattern and applying dipole selection rules to normal-emission ARUPS spectrum, we found that TTC molecules lie on the Cu(100) substrate with their C—C—C planes and alkyl-chain axes parallel to the Cu[110] direction. We also measured the take-off angle θ dependence of the ARUPS spectra with a fixed incident photon energy for this sample [mode (b)], and found that the observed spectra show a one-dimensional intramolecular energy-band dispersion for the wave vector parallel to the surface. The experimentally observed band structure showed excellent correspondence with the results of reported calculation. The reported band structures derived from an end-on oriented sample also show good correspondence with our data, indicating that the assumption of free-electron-like final state was reasonable, and the estimated value of the inner potential V_0 in this report was a good estimation.

We also simulated the angular dependence of the photoemission intensity and peak shifts with theoretical calculations based on the IAC approximation combined with *ab initio* MO calculations. The obtained results showed excellent agreement with the observed spectra, supporting our conclusions for the orientation of the TTC film from LEED and selection rules, and allowed a detailed analysis of the energy dispersion relation. These results also verified the reliability of theoretical simulation with the IAC/MO approximation. This type of measurement combined with the IAC/MO approximation will extend the possibility to investigate the energy-band dispersion relation of various polymers by using a parallel-oriented oligomer film.

ACKNOWLEDGMENTS

The authors thank Professor Nobuhiro Kosugi of Institute for Molecular Science for the program of *ab initio* MO cal-

culation, and Toshiaki Noda of the Faculty of Science, Nagoya University, for constructing the quartz cell of the evaporation source. One of the authors (D.Y.) expresses thanks for the support of the Japan Society for the Promotion of Science for Japanese Junior Scientists. This work was supported in part by Grants-in-Aid for Scientific Research from the Ministry of Education, Science, Sports, and Culture of Japan (Grants Nos. 07CE2004 and 10440205) and Venture Business Laboratory Project ''Advanced Nanoprocess Technologies'' at Nagoya University. This work was performed as a Joint Studies Program of the UVSOR facility of Institute for Molecular Science (No. 6-H217).

[1] *Angle-Resolved Photoemission—Theory and Current Applications*, edited by S. D. Kevan, Studies in Surface Science and Catalysis Vol. 74 (Elsevier, Amsterdam, 1992).
[2] K. Seki, S. Hashimoto, N. Sato, Y. Harada, K. Ishii, H. Inokuchi, and J. Kanabe, J. Chem. Phys. **66**, 3644 (1977).
[3] S. Hüfner, in *Photoelectron Spectroscopy*, edited by M. Cardona, P. Flude, K. von Klitzing, and H. J. Queisser, Solid-State Sciences Vol. 89 (Springer, Berlin, 1995).
[4] K. Seki, in *Optical Techniques to Characterize Polymer Systems*, edited by H. Baessler (Elsevier, Amsterdam, 1989).
[5] K. Seki, U. Karlsson, R. Engelhardt, and E. E. Koch, Chem. Phys. Lett. **103**, 343 (1984).
[6] N. Ueno, W. Gädeke, E. E. Koch, R. Engelhardt, R. Dudde, L. Laxhuber, and H. Möhwald, J. Mol. Electron. **1**, 19 (1985).
[7] H. Fujimoto, T. Mori, H. Inokuchi, N. Ueno, K. Sugita, and K. Seki, Chem. Phys. Lett. **141**, 485 (1987).
[8] K. Seki, N. Ueno, U. O. Karlson, R. Engelhardt, and E. E. Koch, Chem. Phys. **105**, 247 (1986).
[9] N. Ueno, K. Seki, N. Sato, H. Fujimoto, T. Kuramochi, K. Sugita, and H. Inokuchi, Phys. Rev. B **41**, 1176 (1990).
[10] Ch. Zubrägel, F. Schneider, M. Neumann, G. Hähner, Ch. Wöll, and M. Grunze, Chem. Phys. Lett. **219**, 127 (1994).
[11] N. Ueno, K. Sugita, K. Seki, and H. Inokuchi, Phys. Rev. B **34**, 6386 (1986).
[12] N. Ueno and K. Sugita, Phys. Rev. B **42**, 1659 (1990).
[13] W. R. Salaneck, M. Fahlman, C. Lapersonne-Meyer, J.-L. Fave, M. Schott, M. Lögdlund, and J. L. Brédas, Synth. Met. **67**, 309 (1994).
[14] H. J. Stoltz, L. Ley, T. Grandke, and J. Azoulay, in *Photoemission in Solid II*, edited by L. Ley and M. Cardona (Springer-Verlag, Berlin, 1979), Chap. 5, Sec. 6.
[15] L. E. Firment and G. A. Somorjai, J. Chem. Phys. **69**, 3940 (1978).
[16] L. E. Firment and G. A. Somorjai, J. Chem. Phys. **66**, 2901 (1977).
[17] P. S. Bagus, K. Weiss, A. Schertel, Ch. Wöll, W. Braun, C. Hellwig, and C. Jung, Chem. Phys. Lett. **248**, 129 (1996).
[18] E. Ito, H. Oji, H. Ishii, K. Oichi, Y. Ouchi, and K. Seki, Chem. Phys. Lett. **287**, 137 (1998).
[19] H. Ozaki and Y. Harada, J. Am. Chem. Soc. **112**, 5735 (1990).
[20] B. Venkataraman, J. J. Breen, and G. W. Flynn, J. Phys. Chem. **99**, 6608 (1995).
[21] J. P. Rabe and S. Buchholz, Science **253**, 424 (1991).
[22] K. Morishige, Y. Takami, and Y. Yokota, Phys. Rev. B **48**, 8277 (1993).
[23] M. Yamamoto, Y. Sakurai, Y. Hosoi, H. Ishii, E. Ito, K. Kajikawa, Y. Ouchi, and K. Seki, Surf. Sci. **427-428**, 388 (1999).
[24] M. Yamamoto (unpublished).
[25] Y. Hosoi (unpublished).
[26] A. V. Teplyakov, B. E. Bent, J. Eng, Jr., and J. G. Chen, Surf. Sci. Lett. **399**, L342 (1998).
[27] R. Dudde and B. Reihl, Chem. Phys. Lett. **196**, 91 (1992).
[28] J. Weckesser, D. Fuhrmann, K. Weiss, Ch. Wöll, and N. V. Richardson, Surf. Rev. Lett. **2**, 209 (1997).
[29] R. G. Nuzzo, E. M. Korenic, and L. H. Dubois, J. Chem. Phys. **93**, 767 (1990).
[30] G. Hähner, M. Kinzler, C. Thümmler, Ch. Wöll, and M. Grunze, J. Vac. Sci. Technol. A **10**, 2758 (1992).
[31] W. D. Grobman, Phys. Rev. B **17**, 4573 (1978).
[32] N. J. Schevchik, J. Phys. C **11**, 3521 (1978).
[33] N. Ueno, K. Suzuki, S. Hasegawa, K. Kamiya, K. Seki, and H. Inokuchi, J. Chem. Phys. **99**, 7169 (1993).
[34] K. K. Okudaira, S. Hasegawa, H. Ishii, K. Seki, Y. Harada, and N. Ueno, J. Appl. Phys. **85**, 6453 (1999).
[35] S. Hasegawa, S. Tanaka, Y. Yamashita, H. Inokuchi, H. Fujimoto, K. Kamiya, K. Seki, and N. Ueno, Phys. Rev. B **48**, 2596 (1993).
[36] S. Hasegawa, T. Mori, K. Imaeda, S. Tanaka, Y. Yamashita, H. Inokuchi, H. Fujimoto, K. Seki, and N. Ueno, J. Chem. Phys. **100**, 6969 (1994).
[37] N. Ueno, A. Kitamura, K. K. Okudaira, T. Miyamae, Y. Harada, S. Hasegawa, H. Ishii, H. Inokuchi, T. Fujikawa, T. Miyazaki, and K. Seki, J. Chem. Phys. **107**, 2079 (1997).
[38] S. Hasegawa, H. Inokuchi, K. Seki, and N. Ueno, J. Electron Spectrosc. Relat. Phenom. **78**, 391 (1996).
[39] Y. Azuma, T. Hasebe, T. Miyamae, K. K. Okudaira, Y. Harada, K. Seki, E. Morikawa, V. Saile, and N. Ueno, J. Synchrotron Radiat. **5**, 1044 (1998).
[40] S. Narioka, H. Ishii, K. Edamatsu, K. Kamiya, S. Hasegawa, T. Ohta, N. Ueno, and K. Seki, Phys. Rev. B **52**, 2362 (1995).
[41] S. Hasegawa, T. Miyamae, K. Yakushi, H. Inokuchi, K. Seki, and N. Ueno, Phys. Rev. B **58**, 4927 (1998).
[42] K. K. Okudaira, E. Morikawa, S. Hasegawa, P. T. Sprunger, V. Saile, K. Seki, Y. Harada, and N. Ueno, J. Electron Spectrosc. Relat. Phenom. **88-91**, 913 (1998).
[43] T. Miyamae, N. Ueno, S. Hasegawa, Y. Saito, T. Yamamoto, and K. Seki, J. Chem. Phys. **110**, 2552 (1999).
[44] N. Ueno, Y. Azuma, M. Tsutsui, K. K. Okudaira, and Y. Harada, Jpn. J. Appl. Phys. **37**, 4979 (1998).
[45] S. Narioka, H. Ishii, D. Yoshimura, M. Sei, Y. Ouchi, S. Hasegawa, T. Miyazaki, Y. Harima, K. Yamashita, and K. Seki, Appl. Phys. Lett. **67**, 1899 (1995).
[46] D. Yoshimura, H. Ishii, S. Narioka, M. Sei, Y. Ouchi, S. Hasegawa, T. Miyazaki, Y. Harima, K. Yamashita, and K. Seki, Synth. Met. **86**, 2399 (1997).
[47] K. Sugiyama, D. Yoshimura, T. Miyamae, T. Miyazaki, H. Ishii, Y. Ouchi, and K. Seki, J. Appl. Phys. **83**, 4928 (1998).
[48] H. Ishii, K. Sugiyama, D. Yoshimura, E. Ito, Y. Ouchi, and K. Seki, IEEE J. Sel. Top. Quantum Electron. **4**, 24 (1998).
[49] H. Ishii, E. Morikawa, S. J. Tang, D. Yoshimura, E. Ito, K. Okudaira, T. Miyamae, S. Hasegawa, P. T. Sprunger, N. Ueno, K.

Seki, and V. Saile, J. Electron Spectrosc. Relat. Phenom. **101-103**, 559 (1999).
[50] K. Seki, H. Nakagawa, K. Fukui, E. Ishiguro, R. Kato, T. Mori, K. Sakai, and M. Watanabe, Nucl. Instrum. Methods Phys. Res. A **246**, 264 (1986).
[51] S. Narioka, Ph.D. thesis, Nagoya University, 1996.
[52] E. Ito, Ph.D. thesis, Nagoya University, 1997.
[53] V. Vand, Acta Crystallogr. **6**, 797 (1953).
[54] J. J. Ritsko, J. Chem. Phys. **70**, 5343 (1979).
[55] N. Ueno, K. Sugita, O. Koga, and S. Suzuki, Jpn. J. Appl. Phys. **22**, 1613 (1983).
[56] J. B. Pendry, in *Low Energy Electron Diffraction* (Academic, London, 1974).
[57] F. Harman and S. Skillman, in *Atomic Structure Calculations* (Prentice-Hall, Englewood Cliffs, NJ, 1963).
[58] N. Kosugi, Program GSCF3, Library Program, The Computer Center, The University of Tokyo, Tokyo, Japan, 1985; N. Kosugi and H. Kuroda, Chem. Phys. Lett. **74**, 490 (1980).
[59] J. J. Pireaux, S. Svensson, E. Basilier, P.-A. Malmqvist, U. Gelius, R. Caudano, and K. Siegbahn, Phys. Rev. A **14**, 2133 (1976).
[60] K. Seki, N. Sato, and H. Inokuchi, Chem. Phys. **178**, 207 (1993).
[61] G. Ertl and J. Küppers, in *Low Energy Electrons and Surface Chemistry*, edited by H. F. Ebel, Monographs in Modern Chemistry Vol. 4 (Verlag Chemie, Weinheim, 1974).
[62] S. Fitzwater and L. S. Bartell, J. Am. Chem. Soc. **98**, 8338 (1976).
[63] L. Pauling, in *The Nature of the Chemical Bond*, 3rd ed. (Cornell University Press, Ithaca, NY, 1960).
[64] E. Clementi, J. Chem. Phys. **54**, 2492 (1971).
[65] E. Cartier, P. Pfluger, J. J. Pireaux, and M. R. Vilar, Appl. Phys. A: Solids Surf. **44**, 43 (1987).
[66] M. C. Tobin, J. Mol. Spectrosc. **4**, 349 (1960).
[67] W. L. McCubbin, Phys. Status Solidi **16**, 289 (1966).
[68] W. L. McCubbin and I. D. C. Gurney, J. Chem. Phys. **43**, 983 (1965).
[69] A. Karpfen, J. Chem. Phys. **75**, 238 (1981).
[70] M. Deleuze, and L. S. Cederbaum, J. Chem. Phys. **105**, 7583 (1996), and references therein.
[71] J. Sun and R. J. Bartlett, Phys. Rev. Lett. **77**, 3669 (1996), and references therein.
[72] See for example, N. C. Greenham and R. H. Friend, Solid State Phys. **49**, 1 (1995).
[73] B. A. Sexton and A. E. Hughes, Surf. Sci. **140**, 227 (1984).
[74] A. Zangwill, in *Physics at Surfaces* (Cambridge University Press, Cambridge, 1988), Chap. 8.
[75] H. Ishii, K. Sugiyama, E. Ito, and K. Seki, Adv. Mater. **11**, 605 (1999).